SPECTROSCOPY OF HIGH-REDSHIFT SUPERNOVAE FROM THE ESSENCE PROJECT: THE FIRST FOUR YEARS

R. J. Foley[1,2,21], T. Matheson[3], S. Blondin[2,4], R. Chornock[1], J. M. Silverman[1], P. Challis[2], A. Clocchiatti[5], A. V. Filippenko[1], R. P. Kirshner[2], B. Leibundgut[4], J. Sollerman[6,7], J. Spyromilio[4], J. L. Tonry[8], T. M. Davis[7,9], P. M. Garnavich[10], S. W. Jha[1,11,12], K. Krisciunas[13], W. Li[1], G. Pignata[14], A. Rest[15,16], A. G. Riess[17,18], B. P. Schmidt[19], R. C. Smith[16], C. W. Stubbs[2,15], B. E. Tucker[19], AND W. M. Wood-Vasey[2,20]

[1] Department of Astronomy, University of California, Berkeley, CA 94720-3411, USA; rfoley@cfa.harvard.edu
[2] Harvard-Smithsonian Center for Astrophysics, 60 Garden Street, Cambridge, MA 02138, USA
[3] National Optical Astronomy Observatory, 950 North Cherry Avenue, Tucson, AZ 85719-4933, USA
[4] European Southern Observatory, Karl-Schwarzschild-Strasse 2, D-85748 Garching, Germany
[5] Pontificia Universidad Católica de Chile, Departamento de Astronomía y Astrofísica, Casilla 306, Santiago 22, Chile
[6] Dark Cosmology Centre, Niels Bohr Institute, University of Copenhagen, Juliane Maries Vej 30, DK-2100 Copenhagen Ø, Denmark
[7] Department of Astronomy, Stockholm University, AlbaNova, 10691 Stockholm, Sweden
[8] Institute for Astronomy, University of Hawaii, 2680 Woodlawn Drive, Honolulu, HI 96822, USA
[9] Department of Physics, University of Queensland, QLD, 4072 Australia
[10] Department of Physics, University of Notre Dame, 225 Nieuwland Science Hall, Notre Dame, IN 46556-5670, USA
[11] Department of Physics and Astronomy, Rutgers, the State University of New Jersey, 136 Frelinghuysen Road, Piscataway, NJ 08854, USA
[12] Kavli Institute for Particle Astrophysics and Cosmology, Stanford Linear Accelerator Center, 2575 Sand Hill Road, MS 29, Menlo Park, CA 94025, USA
[13] Department of Physics, Texas A&M University, College Station, TX 77843-4242, USA
[14] Departamento de Astronomia, Universidad de Chile, Casilla 36-D, Santiago, Chile
[15] Department of Physics, Harvard University, 17 Oxford Street, Cambridge, MA 02138, USA
[16] National Optical Astronomy Observatory / Cerro Tololo Inter-American Observatory, Casilla 603, La Serena, Chile
[17] Space Telescope Science Institute, 3700 San Martin Drive, Baltimore, MD 21218, USA
[18] Johns Hopkins University, 3400 North Charles Street, Baltimore, MD 21218, USA
[19] The Research School of Astronomy and Astrophysics, The Australian National University, Mount Stromlo and Siding Spring Observatories, via Cotter Road, Weston Creek, PO 2611, Australia
[20] Department of Physics and Astronomy, University of Pittsburgh, 100 Allen Hall, Pittsburgh, PA 15260, USA

ABSTRACT

We present the results of spectroscopic observations from the ESSENCE high-redshift supernova (SN) survey during its first four years of operation. This sample includes spectra of all SNe Ia whose light curves were presented by Miknaitis et al. and used in the cosmological analyses of Davis et al. and Wood-Vasey et al. The sample represents 273 hr of spectroscopic observations with 6.5–10 m class telescopes of objects detected and selected for spectroscopy by the ESSENCE team. We present 184 spectra of 156 objects. Combining this sample with that of Matheson et al., we have a total sample of 329 spectra of 274 objects. From this, we are able to spectroscopically classify 118 Type Ia SNe. As the survey has matured, the efficiency of classifying SNe Ia has remained constant while we have observed both higher-redshift SNe Ia and SNe Ia farther from maximum brightness. Examining the subsample of SNe Ia with host-galaxy redshifts shows that redshifts derived from only the SN Ia spectra are consistent with redshifts found from host-galaxy spectra. Moreover, the phases derived from only the SN Ia spectra are consistent with those derived from light-curve fits. By comparing our spectra to local templates, we find that the rate of objects similar to the overluminous SN 1991T and the underluminous SN 1991bg in our sample are consistent with that of the local sample. We do note, however, that we detect no object spectroscopically or photometrically similar to SN 1991bg. Although systematic effects could reduce the high-redshift rate we expect based on the low-redshift surveys, it is possible that SN 1991bg-like SNe Ia are less prevalent at high redshift.

Key words: distance scale – galaxies: distances and redshifts – supernovae: general

Online-only material: extended figure set, machine-readable and VO tables, color figures

1. INTRODUCTION

A decade after the observations of high-redshift Type Ia supernovae (SNe Ia) caused a sea change in cosmology, indicating that the expansion rate of the universe is currently accelerating (Riess et al. 1998; Perlmutter et al. 1999; see Filippenko 2005 for a review), we are still far from understanding the nature of the "dark energy" that causes this accelerated expansion. Recent high-redshift SN Ia surveys, using the large and normalized peak luminosities of SNe Ia, have focused on measuring the equation-of-state parameter of the dark energy, $w = P/(\rho c^2)$, currently constraining it to ~10% (Astier et al. 2006; Riess et al. 2007; Wood-Vasey et al. 2007; Kowalski et al. 2008).

The determination of the expansion history of the universe with SNe Ia is performed by measuring the luminosity distance as a function of redshift. A relationship between the light-curve shape of an SN Ia and its luminosity is used to obtain precise luminosity distances (e.g., Phillips 1993; Jha et al. 2007; Guy et al. 2007). The redshift of the object is typically found through spectroscopy of the SN by cross-correlating with low-redshift template spectra or its host galaxy. Although photometry alone can be powerful (e.g., Barris & Tonry 2004;

Poznanski et al. 2007), only spectroscopy can currently provide the accurate classification and redshifts necessary for estimating cosmological parameters.

Besides providing the redshift for each object, spectroscopy allows detailed studies of the physics of high-redshift SNe Ia. A critical aspect of high-redshift SN Ia surveys is to only include SNe Ia, and not other transient objects, in their final analysis. Since the optical spectra of SNe Ia are distinct from most transient phenomena, spectroscopy provides a consistent and precise method for determining the nature of each transient (see Filippenko 1997 for a review of SN spectroscopy). Furthermore, with high-redshift SN Ia spectra one can compare the physical properties of the objects with their low-redshift counterparts (e.g., Blondin et al. 2006; Balland et al. 2007; Garavini et al. 2007; Bronder et al. 2008; Ellis et al. 2008; Foley et al. 2008).

In order to measure w to $\lesssim 10\%$, the Equation of State: SupErNovae trace Cosmic Expansion (ESSENCE) team has concluded a six-year NOAO survey project using the CTIO 4 m telescope and the MOSAIC II camera with the intention of discovering and following ∼200 SNe Ia over the redshift range of $0.2 < z < 0.8$ (Miknaitis et al. 2007). During the first four years of the ESSENCE survey, which observed approximately October through December, several hundred transient objects were detected (Miknaitis et al. 2007). As most of these objects were relatively faint ($R > 21$ mag), a large amount of telescope time at 6.5–10 m telescopes was required for spectroscopic follow-up observations. Despite being awarded approximately 100 nights at these facilities over the first four years of the survey, we were still not able to obtain a spectrum of every candidate object (Matheson et al. 2005).

However, during the first 12 search months (ESSENCE searched three months per year), we were able to classify 121 SNe Ia. In this paper, we present the spectra of all spectroscopic targets observed during the first four years of the ESSENCE survey. This sample, which updates and supersedes the analysis of Matheson et al. (2005) for the spectroscopy of the first two years of the ESSENCE survey, includes all SNe Ia presented by Miknaitis et al. (2007) and used in the analysis of Wood-Vasey et al. (2007) and Davis et al. (2007). We discuss our observations in Section 2. The classification scheme presented by Matheson et al. (2005), Miknaitis et al. (2007), and Blondin & Tonry (2007) is updated in Section 3 (the method is similar to that presented by Miknaitis et al. 2007). In Section 4, we discuss the properties of our sample, and we summarize our conclusions in Section 5.

2. OBSERVATIONS

Over the first four years of the ESSENCE survey, we detected several thousand transient objects. Since we did not have adequate observing time at large telescopes to follow each transient spectroscopically, we prioritized the objects by a combination of likelihood to be a SN Ia, observational ease, and, occasionally, likely redshift and phase relative to maximum light. These criteria were all determined from our search images, using features such as color and offset from the host galaxy. In particular, the likelihood of an object being a SN Ia is deduced from an approximate photo-z of its host, its $R-I$ color (Tonry et al. 2003), and its rise time. Objects which had particularly blue colors were considered more likely to be core-collapse SNe, while objects with a slow rise time were more likely to be active galactic nuclei (AGNs) or other transients. Further details about the target selection can be found in Matheson et al. (2005) and Miknaitis et al. (2007).

Spectroscopic observations of ESSENCE targets were obtained at a wide variety of telescopes: the Keck I and II 10 m telescopes, the European Southern Observatory 8.2 m Very Large Telescope (ESO VLT), the Gemini North and South 8 m telescopes, the Magellan Baade and Clay 6.5 m telescopes, and the MMT 6.5 m telescope. The spectrographs used were LRIS (Oke et al. 1995) with Keck I, DEIMOS (Faber et al. 2003) with Keck II, FORS1 (Appenzeller et al. 1998) with the VLT, GMOS (Hook et al. 2004) with Gemini (North and South), IMACS (Dressler et al. 2006) with Baade, LDSS2 (Allington-Smith et al. 1994) and LDSS3[22] with Clay, and the Blue Channel (Schmidt et al. 1989) with MMT. Nod-and-shuffle techniques (Glazebrook & Bland-Hawthorn 2001) were used with GMOS (North and South) and some IMACS observations to improve sky subtraction in the red portion of the spectrum. A single spectrum was obtained with the FAST spectrograph (Fabricant et al. 1998) mounted on the Tillinghast 1.5 m telescope at the F. L. Whipple Observatory.

Standard CCD processing and spectrum extraction were accomplished with IRAF.[23] Most of the data were extracted using the optimal algorithm of Horne (1986); for the ESO VLT data, an alternative extraction method based on Richardson–Lucy restoration (Blondin et al. 2005) was employed. Low-order polynomial fits to calibration-lamp spectra were used to establish the wavelength scale. Small adjustments derived from night-sky lines in the object frames were applied. We employed our own IDL routines to flux calibrate the data and remove telluric lines using the well exposed continua of the spectrophotometric standards (Wade & Horne 1988; Foley et al. 2003).

The photometric data were obtained on the NOAO Blanco 4 m telescope with the MOSAIC II imaging camera. The light curves for the SNe Ia are available online[24] (Miknaitis et al. 2007).

In Table 1, we present a full list of our observations (date of observation, telescope/instrument, and exposure times). We also include information about the nature of each object (object classification, redshift, and, if an SN Ia, phase and light-curve shape). We present the spectra from 2004 and 2005 in Figures 1–6 (All additional spectra are available in the online version of the journal). For each SN Ia, we plot both the spectrum of the SN as well as the best-fit SNID (Blondin & Tonry 2007) template spectrum.

3. OBJECT CLASSIFICATION

As all cosmological results resulting from the ESSENCE survey depend on having an uncontaminated sample of SNe Ia, we must pay particular attention to proper object classification. SN classification is based on the optical spectrum (Filippenko 1997; Turatto 2003). Type II SNe are characterized by the presence of obvious hydrogen lines, while Type I SNe lack hydrogen. Type I SNe are further distinguished by the presence of He (Type Ib), strong Si II λ6355 (Type Ia), or the lack (or weak presence) of both (Type Ic). The velocity of the SN ejecta causes the features to be blueshifted, with the Si II λ6355 feature typically being observed in absorption at ∼6150 Å.

Table 1
Essence Spectroscopic Targets

ESSENCE ID[a]	IAUC ID[b]	UT Date	Telescope	Type[c]	Subtype	z (Gal)[d]	z (SNID)[e]	Template	Phase (SNID) (d)	Phase (LC) (d)	Δ	Disc. Mag.	Exp. (s)
a002.wxc1_04	. . .	2002-12-06.03	VLT	Gal	. . .	0.315	. . .	. . .	. . .	. . .	. . .	. . .	900
b001.wxc1_14	. . .	2002-11-03.23	MMT	Unk	. . .	. . .	. . .	. . .	. . .	. . .	. . .	. . .	1800
b001.wxc1_14	. . .	2002-11-06.27	KII/ESI	Unk	. . .	. . .	. . .	. . .	. . .	. . .	. . .	. . .	1600
b001.wxc1_14	. . .	2002-11-11.32	KI/LRIS	Unk	. . .	. . .	. . .	. . .	. . .	. . .	. . .	. . .	1800
b001.wxc1_14	. . .	2002-12-05.26	GMOS	Unk	. . .	. . .	. . .	. . .	. . .	. . .	. . .	. . .	2x1800
b002.wxh1_01	. . .	2002-11-01.44	KII/ESI	Star	. . .	. . .	. . .	. . .	. . .	. . .	. . .	. . .	900
b003.wxh1_14	2002iu	2002-11-01.43	KII/ESI	Ia	norm	. . .	0.115 (0.005)	1999ee	−3.8 (3.2)	. . .	. . .	. . .	600
b004.wxt2_06	2002iv	2002-11-02.45	KII/ESI	Ia	91T	0.231	0.226 (0.006)	2005eq	−4.9 (1.6)	. . .	. . .	. . .	1200
b005.wxd1_11	2002iw	2002-11-03.16	MMT	Gal	. . .	0.205	. . .	. . .	. . .	. . .	. . .	. . .	3x1800
b005.wxd1_11	2002iw	2002-11-06.32	KII/ESI	Gal	. . .	0.205	. . .	. . .	. . .	. . .	. . .	. . .	1800

Notes.
[a] ESSENCE internal identification. The first letter indicates the month in the observing season. This is followed by a sequential number as targets are discovered. The remaining letters and numbers show the specific ESSENCE field where the object was located.
[b] Note that not all objects judged to be SNe have official International Astronomical Union names.
[c] Our best guess as to classification of the object. "Ia?" indicates a lack of certainty in the identification as an SN Ia. Objects marked "Unk" are unknown. N.S. indicates that the telescope was pointed to the object, but no exposure was taken or the exposure contained no signal.
[d] Redshift measured from narrow emission or absorption lines from the host galaxy. All galactic redshift errors are < 0.001.
[e] Redshift measured from the SN spectrum by SNID.
(This table is available in its entirety in machine-readable and Virtual Observatory (VO) forms in the online journal. A portion is shown here for guidance regarding its form and content.)
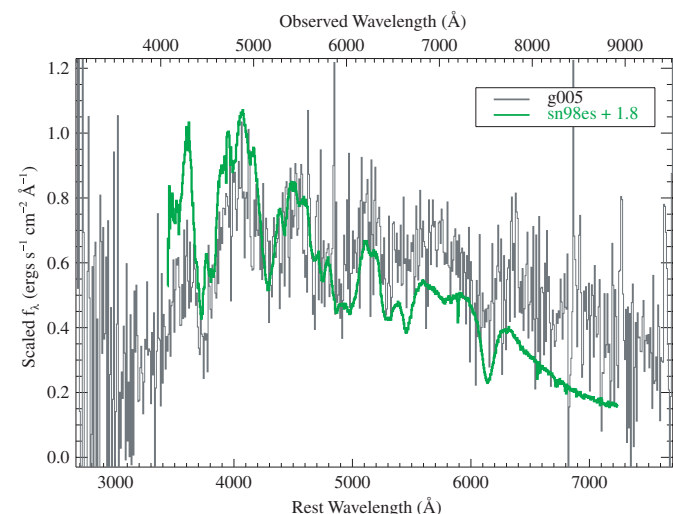

Figure 1. Spectrum of g005 at $z = 0.20$ compared to SN 1998es, an SN 1991T-like SN Ia, at $t = 1.8$ d relative to B-band maximum. Differences in the continuum shape are ignored by SNID, which removes a pseudocontinuum from the spectra before cross-correlation.

(An extended version of this color figure is available in the online journal.)

Figure 2. Spectrum of g043 at $z = 0.187$ compared to SN 1999em, an SN II-P. Differences in the continuum shape are ignored by SNID, which attempts to remove a pseudocontinuum by fitting a low-order polynomial to the spectra before cross-correlation.

With fully calibrated spectra, we can attempt to classify the object by physical origin. SNe, having broad ($\sim$10,000 km s^{-1}) spectral features, are very distinct from AGNs, galaxies, stars, and other astrophysical objects. However, it can occasionally be difficult to distinguish among SN types. High-redshift SN spectra typically have low signal-to-noise ratio (S/N) and considerable host-galaxy contamination, while lacking the Si II λ6355 feature (which is redshifted outside the optical range), which can make differentiating between SN types quite difficult. Accordingly, we have implemented the SNID algorithm (Blondin & Tonry 2007) to determine SN types.

SNID correlates an input spectrum with a large database of template spectra at zero redshift. These include nearby ($z < 0.1$) SNe of all types (Ia, Ib, Ic, II), as well as galaxies, AGNs, luminous blue variables (LBVs), and other variable stars (see
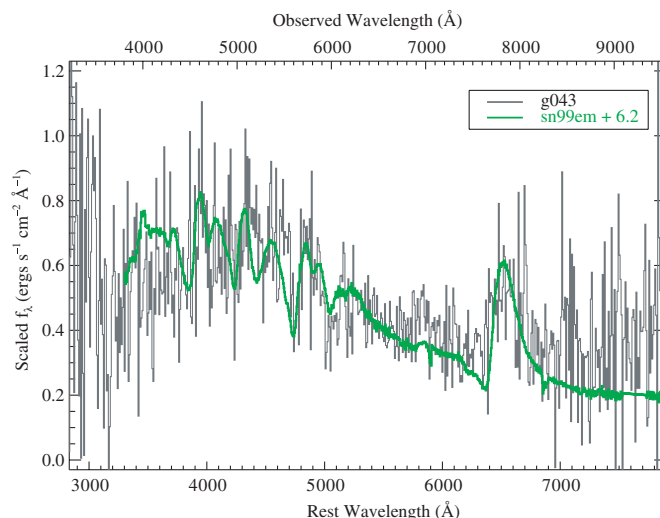
Blondin & Tonry 2007 for the complete database listing). The SNID algorithm has been extensively described by Blondin & Tonry (2007) and already used to determine the type, redshift, and age of ESSENCE SN spectra by Matheson et al. (2005) and Miknaitis et al. (2007), and we refer the reader to these papers for more details (in particular for what is meant by a "good" correlation).

We also attempt to further divide each SN type into subtypes as follows: Ia – Ia-norm, Ia-pec, Ia-91T, Ia-91bg; Ib – Ib-norm, Ib-pec, IIb; Ic – Ic-norm, Ic-pec, Ic-broad; II – IIP, II-87A, IIL, IIn, IIb. "Norm" and "pec" subtypes are used to identify the spectroscopically "normal" and "peculiar" SNe of a given type (see Blondin & Tonry 2007 for a detailed description of each subtype). For SNe Ia, "91T" indicates spectra that resemble those of the overluminous SN 1991T (Filippenko et al. 1992b; Phillips et al. 1992), and also includes SN 1999aa-like objects
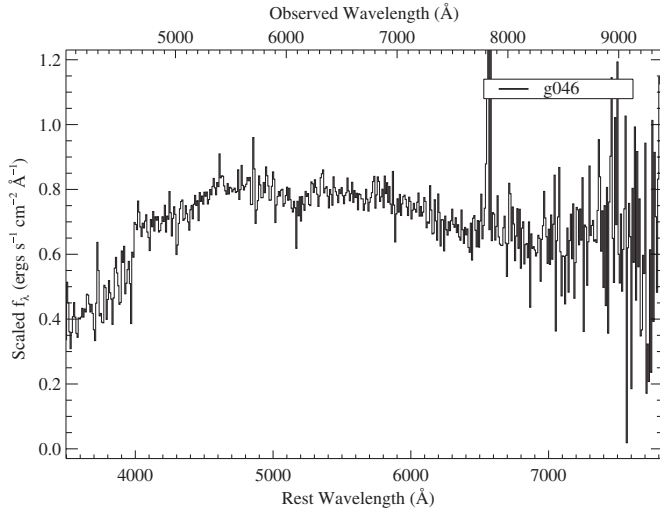
Figure 3. Spectrum of g046 at $z = 0.184$. The spectrum is dominated by galaxy light with no detectable amount of light from a transient object.
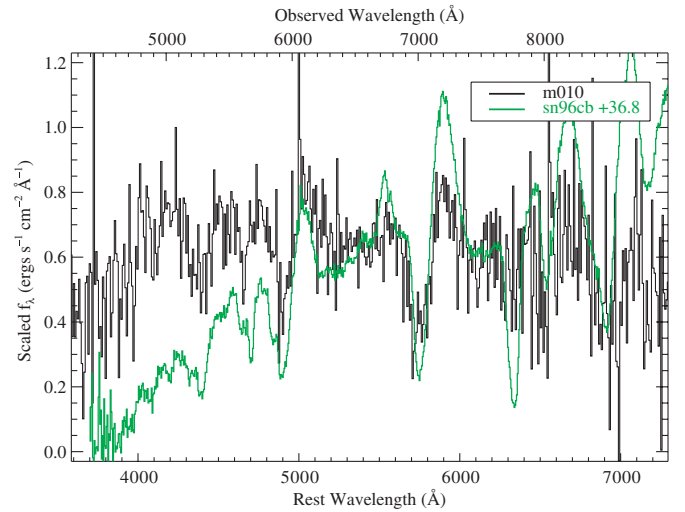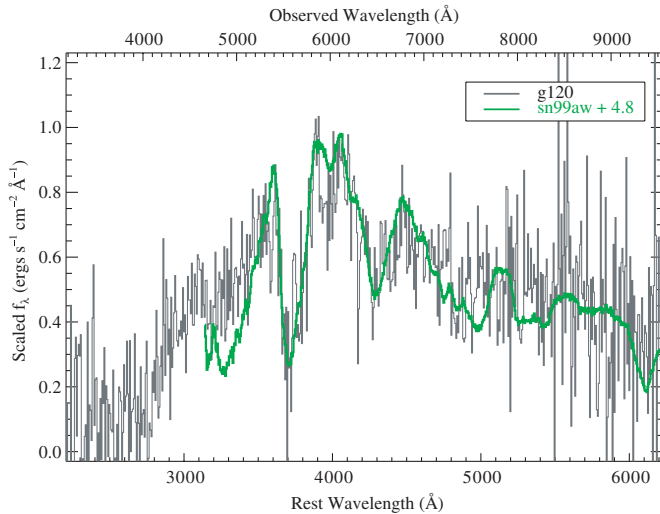

Figure 4. Spectrum of g120 at $z = 0.51$ compared to SN 1999aw, an SN Ia, at $t = 4.8$ d relative to B maximum. We were unable to determine a subtype for g120. Differences in the continuum shape are ignored by SNID, which attempts to remove a pseudocontinuum by fitting a low-order polynomial to the spectra before cross-correlation.

(A color version of this figure is available in the online journal.)

Figure 5. Spectrum of m010 at $z = 0.216$ compared to SN 1996cb, an SN IIb. Differences in the continuum shape are ignored by SNID, which attempts to remove a pseudocontinuum by fitting a low-order polynomial to the spectra before cross-correlation.

(A color version of this figure is available in the online journal.)

Figure 6. Spectrum of p534 at $z = 0.621$ after galaxy subtraction from the superfit routine compared to SN 2003du, an SN Ia. Differences in the continuum shape are ignored by SNID, which removes a pseudocontinuum from the spectra before cross-correlation. Additional figures for all objects listed in Table 1 can be found in the online edition.

(A color version of this figure is available in the online journal.)

(Strolger et al. 2002; Garavini et al. 2004); "91bg" indicates spectra that resemble those of the subluminous SN 1991bg (Filippenko et al. 1992a; Leibundgut et al. 1993), and includes all subluminous objects characterized by a stronger Si II λ5800 line (e.g., SN 1999gh; Matheson et al. 2008). The spectra that correspond to the "Ia-pec" category in this case are those of SN 2000cx-like (Li et al. 2001b) and SN 2002cx-like (Li et al. 2003) events. These classifications correspond roughly to the categories defined by Branch et al. (1993). For Type Ic SNe, "Ic-broad" is used to identify broad-lined SNe Ic (often referred to as "hypernovae" in the literature; see Galama et al. 1998 and Foley et al. 2003 for well known examples), some of which are associated with gamma-ray bursts. The notation adopted for the Type II subtypes is commonly used in the literature. Note that Type IIb SNe (whose spectra evolve from a Type II to a Type Ib, as in SNe 1987K and 1993J; see Filippenko 1988, Filippenko et al. 1993, and Matheson et al. 2000) are included both in the
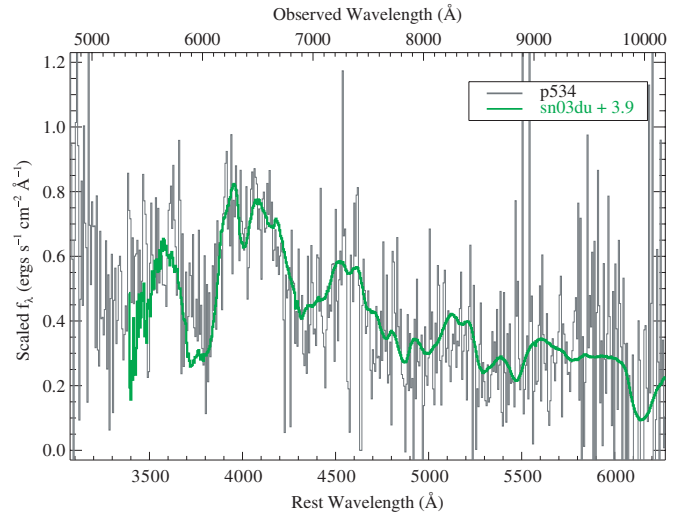
"Ib" and "II" types. All non-SN templates are grouped in the "NotSN" type. We are unable to determine a specific subtype for many objects.

We classify the input spectra in a similar manner to that outlined by Miknaitis et al. (2007). More specifically, we execute four SNID runs to separately determine the type, subtype, redshift, and age of the input spectrum as follows.

1. Type: the input spectrum is asserted to be of a given type when the fraction of "good" correlations that correspond to this type exceeds 50%. In addition, we require the best-match SN template to be of the same type. When the redshift is known beforehand (from narrow emission or absorption lines associated with the host galaxy), we force SNID to only look for correlations at this redshift (± 0.02). If SNID

determines the type of the input spectrum, an attempt is made to determine its subtype.

2. Subtype: to determine the subtype we only consider "good" correlations with template spectra corresponding to the previously determined type. The input spectrum is asserted to be of a given subtype when the fraction of "good" correlations that correspond to this subtype exceeds 50%. In addition, we require the best-match SN template to be of the same subtype. Examples of SNe Ia for which we could and could not determine a subtype are g005 (displayed in Figure 1) and g120 (displayed in Figure 4, respectively. Again, we use the galaxy redshift when available. Regardless of whether SNID determines a subtype, a third run is executed to determine the redshift.

3. Redshift: the SNID redshift corresponds to the median of all "good" template redshifts, while the redshift error is given as the standard deviation of these same redshifts (see Blondin & Tonry 2007 for more details.). If a subtype has been determined, we only consider "good" correlations with template spectra corresponding to this subtype; otherwise, all template spectra of the given type are used. Here no prior information on the galaxy redshift is used. If a redshift is determined in this run, a fourth run is executed to determine the age.

4. Age: the SNID age corresponds to the median of all "good" template ages, while the age error is given as the standard deviation of these same ages. If a subtype has been determined, we only consider "good" correlations with template spectra corresponding to this subtype; otherwise, all template spectra corresponding to the given type are used (as for the redshift determination). The redshift is fixed to the host-galaxy redshift when available, or to the previously determined SNID redshift otherwise (± 0.02). Blondin & Tonry (2007) mention that the age error calculated this way is typically overestimated, but here we make no attempts to compute a more robust age error (as done by Blondin et al. 2008).

Note that we have run SNID on *all* ESSENCE spectra, but only report the SNID output for spectra classified as SNe (Table 1). For all other spectra, we rely on the visual classification by spectroscopy experts within our team. In a few cases, a spectrum not classified as an SN Ia by SNID is found to be consistent with an SN Ia spectrum through visual inspection. For these cases we report a "Ia?" classification. In fact, SNID can sometimes fail to correctly classify an input SN Ia spectrum, mainly because of low S/N or excessive galaxy contamination. Blondin & Tonry (2007) showed that the redshift and age determination with SNID are greatly affected for input spectra that consist of more than 50% galaxy light.

In addition to using SNID, we have applied an alternate technique for SN classification that is based on a χ^2 minimization of fitting an SN spectrum to template spectra with a variable extinction and galaxy contamination (Howell et al. 2005). This method is implemented in the superfit IDL package. The main advantage of the χ^2 minimization technique is that it can classify SNe from spectra that are highly contaminated by galaxy light. One of the main drawbacks of superfit is that it assumes that the continuum of a high-redshift SN Ia must be similar to that of a low-redshift SN Ia. Usually this can be worked around by having a different value for the extinction (which will change the continuum shape of the spectrum even if the value of the "extinction" is not strictly physical) or a different galaxy template. The other main drawback of superfit is that although
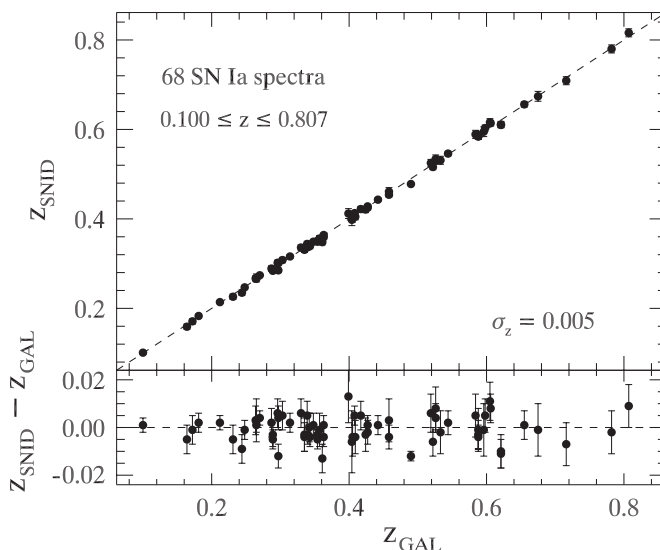

Figure 7. Comparison of redshifts determined from cross-correlations with SN Ia spectral templates using SNID (z_{SNID}) and from narrow lines in the host-galaxy spectrum (z_{GAL}; upper panel). We show the residuals vs. z_{GAL} in the lower panel.

superfit produces a χ^2-like goodness-of-fit parameter, there is no formal evaluation of the uncertainty of any of the derived values (cf., the redshift error in SNID is related to the height of the correlation peak; see Blondin & Tonry 2007).

For both SNID and superfit, as well as any SN spectral fitting routine, the output is dependent on the input parameters such as wavelength range. Because of the different approaches and the various input parameters, it is possible for the fitters to suggest different classifications. However, humans ultimately classify each object, and intelligent inputs to the fitters should yield similar results.

Applying the χ^2 minimization technique to all spectra which were not originally classified by SNID, we obtained several candidate SNe. The superfit package will output a galaxy-subtracted spectrum using a galaxy fraction (and galaxy type) that best matches a given SN template spectrum. Since we have not modeled the robustness of the goodness-of-fit parameter from this technique, we attempted to classify the galaxy-subtracted spectra with SNID. We fit the top five galaxy-subtracted superfit spectra with SNID, looking for a consensus result. For 99 potential candidates, this process yielded one additional SN Ia?(f123), as well as identifying a second-epoch spectrum of an SN Ia (p534; as identified from the other spectrum by SNID) as an SN Ia.

There is some concern that extra degrees of freedom are introduced into our SNID fitting as the superfit packages changes the spectrum by applying an extinction estimate and removing a galaxy spectrum from each input spectrum. However, since SNID normalizes all spectra to have a flat continuum, it is relatively insensitive to reddening.

We have already shown the excellent agreement between the SNID correlation redshift and the redshift of the SN host galaxy (when known) in several publications (Matheson et al. 2005; Miknaitis et al. 2007; Blondin & Tonry 2007; Blondin et al. 2008). Figure 7 again shows that the SNID redshifts agree well with the host-galaxy redshifts, with a dispersion about the one-to-one correspondence of only ~0.006. This figure contains only the SNe Ia where we have an independent measurement of the redshift from a galaxy spectrum.
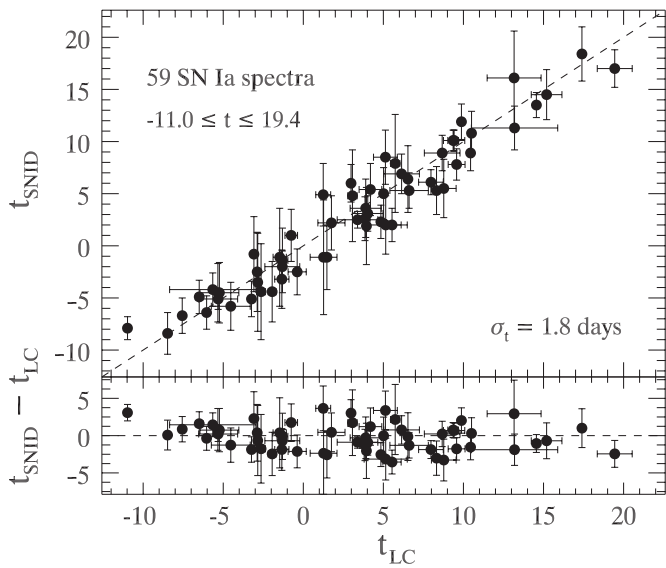
Figure 8. Comparison of SN spectral ages determined using SNID (t_{SNID}) and rest-frame light-curve ages (t_{LC}) of high-z SNe Ia (upper panel). We show the residuals vs. t_{LC} in the lower plot.

The template spectra in the SNID database have ages corrected for the $1/(1+z)$ time-dilation factor expected in an expanding universe (e.g., Blondin et al. 2008), such that SNID determines ages in the SN rest frame. No correction to the age for light-curve width has been made. We can then compare these age estimates (t_{SNID}) with those inferred from a well-sampled light curve (see Miknaitis et al. 2007). We expect a one-to-one correspondence between the light-curve rest-frame age,

$$t_{\text{LC}} = \frac{\Delta t_{\text{obs}}}{1+z}, \qquad (1)$$

and t_{SNID}, where Δt_{obs} is the time difference (in the *observer* frame) between maximum light and the time the spectrum was obtained.

The result is shown in Figure 8. We use all objects with a good light-curve fit and a good SNID age, resulting in a total of 59 SN Ia spectra with rest-frame light-curve ages in the range $-11.0 \leqslant t_{\text{LC}} \leqslant 19.4$ d. The dispersion about the $t_{\text{SNID}} = t_{\text{LC}}$ line is $\sigma_t \approx 2.4$ d, similar to what was found by Blondin & Tonry (2007). We show the residuals versus t_{LC} in the lower plot. The mean residual is approximately -0.7 d. Two points at $t_{\text{LC}} < -10$ d are $\sim 2\sigma$ off the null residual line; this is due to the low number of SN Ia templates at these early phases.

The fact that the SNID correlation redshift and age measurements agree so well with the galaxy redshifts and light-curve ages, respectively, is a strong argument in favor of the similarity of these SNe Ia with local counterparts. This further confirms the results of Matheson et al. (2005), who found that our classification techniques were robust and saw no major indications of SN Ia evolution in our sample. Foley et al. (2008) also see this for the overall sample.

4. HIGH-REDSHIFT SAMPLE

Over the four seasons, we obtained 329 spectra of 274 objects for a total of 273 hr of integration. This has yielded 118 SNe Ia, 9 SNe Ia?, 16 SNe II, 7 SNe Ib/c, 56 galaxies (which may have some SN light in the spectrum, but at an undetectable level), 20 AGNs, 4 stars, and 44 unidentified objects. We provide a detailed assessment of our object classification in Table 2.

Table 2
ESSENCE Spectroscopy Results: The First 4 Years

Type	Year 1	Year 2	Year 3	Year 4	Total
Ia	15	35	30	38	118
Ia?	0	3	2	4	9
II	1	2	6	7	16
Ib/c	1	2	2	2	7
AGN	3	9	0	8	20
Gal	8	11	20	17	56
Star	2	2	0	0	4
Unk/N.S.	6	17	13	8	44
Total	36	81	73	83	274

Notes. Since there were no template observations obtained before Year 1 and no long baseline observations to easily reject AGNs and variable stars, there were fewer high-quality SN Ia candidates in Year 1. As a result, Year 1 had fewer SNe Ia confirmed compared to later years.

Objects with no definitive SNID classification or obvious "by-eye" classification are labeled as "Unk." Objects with no signal in their spectra are labeled as "N.S." Together, objects with these classifications compose the subsample of unidentified objects.

For several objects, we have changed our classification from that published by Matheson et al. (2005). This is mostly the result of an improved version of SNID and additional low-redshift templates for comparison. Additionally, the superfit routine provided several classifications that we were not previously able to determine. In Table 3, we list the objects with different classifications between Matheson et al. (2005) and this work, as well as the dominant reason for the reclassification.

4.1. Survey Efficiency

In order to meet our goal of $\sim$200 SNe Ia over six years, we tried to use our resources as efficiently as possible to detect and classify SNe Ia. Although the ESSENCE survey has been completed, performing an analysis of the efficiency of ESSENCE will provide useful information for the planning of future surveys (e.g., Pan-STARRS and DES).

The process of detecting and classifying SNe Ia can be separated into two tasks: preselecting potential candidates so SNe Ia represent a high percentage of spectroscopic targets, and properly classifying the spectrum of an SN Ia as an SN Ia. The first task is based solely on parameters derived from imaging. The second task relies on having a method of classifying events with high accuracy (such as the SNID algorithm) and having spectra of sufficient quality for that method to determine a classification (which depends on observing conditions, separation from the host galaxy, brightness of the target, exposure time, the spectrograph's wavelength range, etc.).

To examine the synergy of our search with the large-aperture telescope time we used for spectroscopy, we present histograms of our redshift distribution and phase of the first spectrum of each SN Ia in Figures 9 and 10, respectively. From these figures we see that as the survey matured, we were able to detect higher-redshift objects with greater efficiency. The SNe Ia detected during the first two years have an average redshift of 0.38 (and median redshift of 0.41), while the SNe Ia detected during years 3 and 4 have an average redshift of 0.45 (and median redshift of 0.42). We also detected 7 (21) SNe Ia with $z > 0.7$ ($z > 0.6$) in the second two years, while we had detected none (4) in the first two years. Moreover, we were able to detect, observe, and classify SNe Ia at later phases after maximum brightness, when the SNe are fainter.

Table 3
ESSENCE Object Reclassification

ESSENCE ID	IAUC ID	Matheson et al. (2005) Classification	New Classification	Notes
c016.wxm1_04	. . .	AGN	Gal	
c022.wxu2_15	. . .	II?	Ib	IIb subtype
d009.waa6_16	. . .	Gal	Ia	
d120.wcc1_2	. . .	. . .	AGN	Not listed by Matheson et al. (2005)
e141.wdd7_2	. . .	II	Ib	IIb subtype
e143.wdd7_3	. . .	II	Ib	
e149.wdd5_10	2003ks	Ia?	Ia	
f001.wbb7_1	2003kv	Unk	II	
f044.wbb8_8	. . .	Gal	Ia	
f123.wcc1_7	. . .	Gal	Ia?	
f221.wcc4_14	2003lk	Ia?	Gal	
f301.wdd6_1	. . .	Ia?	Ia	
f308.wdd6_10	. . .	Ia?	Ia	
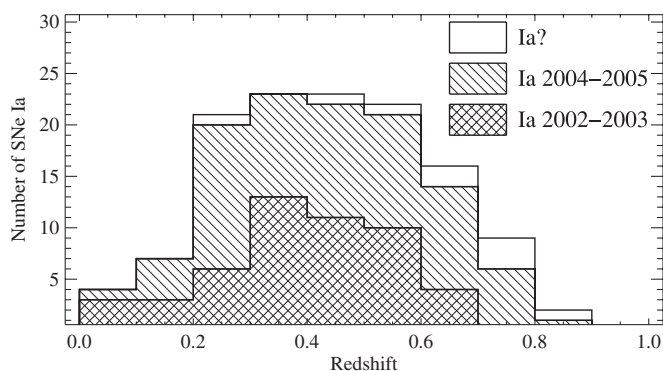
Figure 9. Redshift distribution of spectroscopically identified SNe Ia from the first four years of the ESSENCE survey. The SNe for which we have a high confidence of being of Type Ia (as determined by SNID) are plotted in the hashed region. The open region represents SNe for which we have less confidence and have been classified "SNe Ia?"
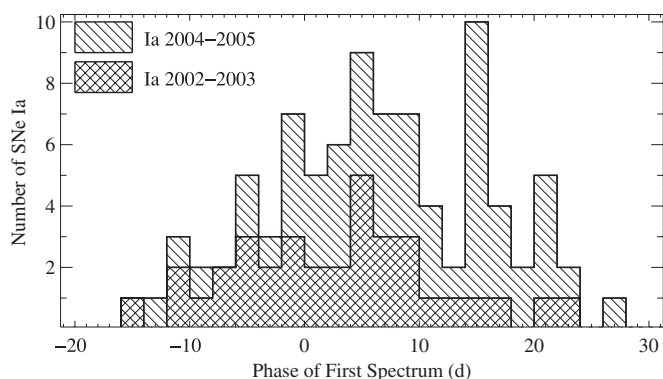

Figure 10. Phase (relative to maximum brightness) distribution of spectroscopically identified SNe Ia from the first four years of the ESSENCE survey and light curves fit by Wood-Vasey et al. (2007).
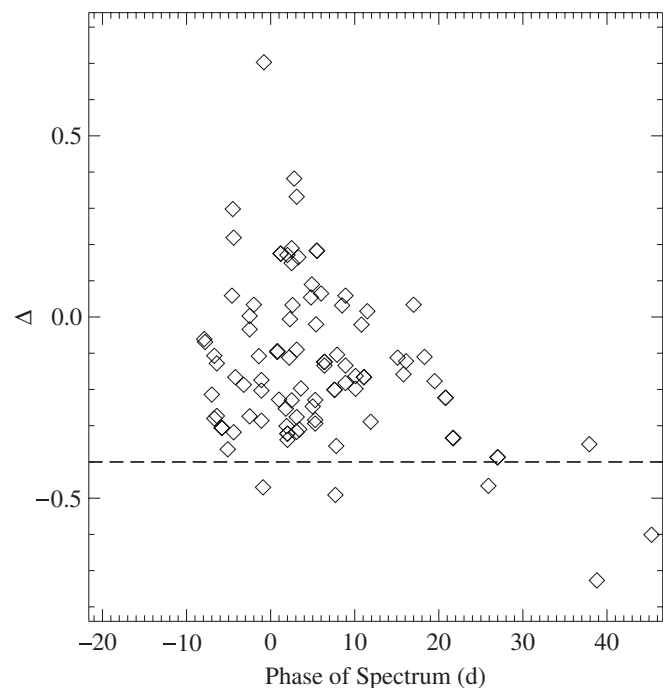
Figure 11 shows that for objects with larger Δ[25] (corresponding to being less luminous), we only obtain spectra near maximum light, while for objects with smaller Δ (corresponding to being more luminous), we obtain spectra for a wide range of phases. Besides being less luminous, high-Δ SNe Ia fade faster than low-Δ SNe Ia, making high-Δ SNe Ia become even fainter relative to low-Δ SNe Ia the farther they are from maximum light. Both of these biases (faintness and faster declining) for high-Δ objects are expected for our sample. However, one may argue that since there are fewer total spectra obtained for older SNe we may be seeing a manifestation of small-number statistics as opposed to a selection effect. To test this hypothesis, we performed a Kolmogorov–Smirnov (K-S) test on the objects with $|t| < 5$ d compared to those with $5 < t < 20$ d and $t > 20$ d; we find the probability that the sets are chosen from different distributions to be 75.6% and 99.9%, respectively. The earlier data are marginally consistent, while the later data are different at a high significance. This is consistent with the expected bias.

In Figure 11, we see that there are five SNe (d058, h311, m022, m043, and m057) with $\Delta < -0.4$, the fiducial Δ limit for the multicolor light-curve shape method (MLCS; Riess et al. 1996; Jha et al. 2007) based on the broadest local SN Ia light curves. There are two reasons for such a low value of Δ:

[25] $M_V(t = 0) = -19.504 \, \mathrm{mag} + 0.736\Delta + 0.182\Delta^2 + 5 \log_{10}(H_0/65)$ (Jha et al. 2007).

Figure 11. Distribution of measured Δ of ESSENCE SNe Ia vs. phase (relative to maximum brightness). Only objects that had light curves fit by Wood-Vasey et al. (2007) have been plotted. The dashed line indicates the Δ limit beyond which MLCS has to extrapolate to fit light curves. As such, objects with $\Delta < -0.4$ should be discounted.
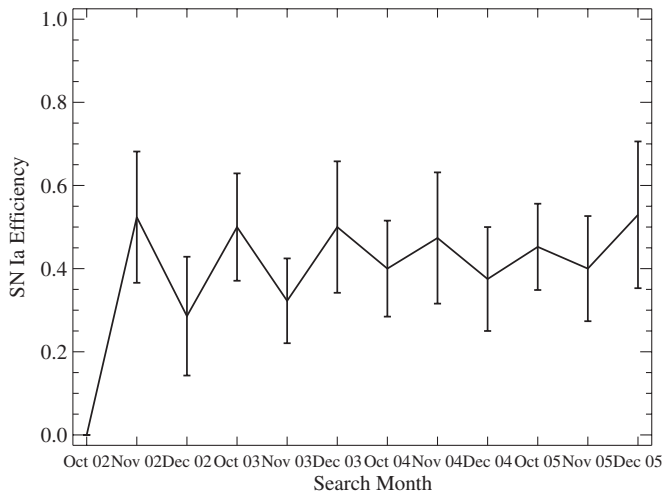
Figure 12. Efficiency of our spectroscopic follow-up observations over the 12 search months in the first four years of ESSENCE. The overall efficiency is 43%.

Figure 13. Efficiency of our spectroscopic follow-up observations over the 12 search months in the first four years of ESSENCE as a function of total spectroscopic exposure time in a given month.

the light curve is broader than any local template, or the light curve is of low quality and the MLCS fit is not robust. Of the five SNe, three (h311, m022, m057) fail the $\chi^2/\mathrm{dof} < 3$ cutoff set by Wood-Vasey et al. (2007). One (m043) has no light-curve points before maximum, so it is difficult to determine if the light curve is truly broad. The final one (d058, with $\Delta = -0.470$) has a well-sampled light curve and is likely to be truly broad. Examining the spectrum, it does not appear that d058 is peculiar; however, the small rest-frame wavelength range (~ 3000–5000 Å) prevents an investigation of important lines such as Si II $\lambda6355$. The first four objects should be ignored since their Δ values are likely to be incorrect. The final object, d058, should be discounted. Although Δ is a well-defined quantity for $\Delta < -0.4$ (indicating the width of a light curve), for such values we must extrapolate beyond the local sample, leading to potentially incorrect distance and luminosity measurements.

We further investigate if we are limited in our number of classified SNe Ia by our search or by our usable time on large-aperture telescopes. In Figure 12, we show our efficiency (given by the ratio of SNe Ia classified to total objects we observed) as a function of search month. However, there are many objects where, after a short exposure, we recognized that it was not an SN Ia. An exposure-time weighted efficiency will be higher than that shown in Figure 12. Throughout the first four years, we consistently classified $\sim 43\%$ of all spectroscopic targets as SNe Ia, perhaps slightly increasing our efficiency with time.

In Figure 13, we show that our efficiency does not change with the amount of spectroscopic time in a given month. This indicates that for a broad range of the number of transients detected per month in our search or for a broad range of spectroscopic follow-up time in a given month, we would obtain about the same ratio of SNe Ia to total spectroscopic targets.

This result is perhaps a little counterintuitive. There are several factors involved. For example, with infinite potential targets from the search, one expects to be able to properly identify excellent candidate SNe Ia, resulting in a higher efficiency. Similarly, with infinite spectroscopic follow-up time, one expects to be able to obtain a spectrum of every transient, resulting in a lower efficiency. But there are other factors. First, when there was a paucity of potential spectroscopic targets, we would obtain additional spectra of already confirmed SNe Ia rather than observe candidates that had a small possibility of
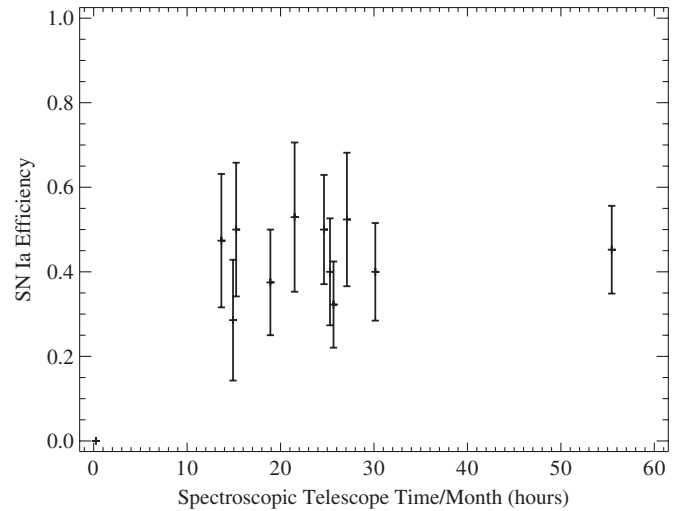
being an SN Ia. Another aspect is the image quality of the search. If a particular month had poor weather or bad seeing at Cerro Tololo, we would typically detect brighter, more isolated objects at lower redshifts. So even if there were fewer objects from which to choose, the objects were typically easier to observe. It is difficult to disentangle all of these effects, but we have shown from our measured efficiencies that they naturally balanced over the first four years of the ESSENCE survey.

Howell et al. (2005) showed that the Supernova Legacy Survey (SNLS) was able to improve their efficiency from 54% to 71% by utilizing multiple colors of the transients and hosts to better predict whether a transient is an SN Ia. The ESSENCE survey, which searched in only R and I, was unable to perform such an analysis. Furthermore, ESSENCE only had R and I photometry for the host galaxies, reducing our ability to determine precise host-galaxy photo-z values. Obviously, if spectroscopic efficiency is a priority, future surveys should have many-filter observations of transients and host galaxies. Additionally, having multiple colors of SNe Ia will greatly improve the measurement of SN colors and dust extinction, which in turn should improve SN distances.

Although we have been able to reduce the number of persistent transients (AGNs, variable stars) observed spectroscopically, we still observed seven AGNs in year 4 (compared to 3, 9, and 0 for years 1, 2, and 3). These objects were selected for spectroscopic observation despite some indications that they were AGNs. This can be attributed to a human error, and having more humans vet the candidates would help prevent such future observations.

Finally, if we remove all transients which are definitely not SNe Ia (i.e., those objects that have spectra which identify them as other types of transient objects), we can determine how successful our spectroscopic classification would have been if we had fewer contaminants. Figure 14 shows the ratio of the number of SNe Ia to the number of total objects which may be SNe Ia (those classified as SNe Ia, SNe Ia?, Gal, Unk, or N.S.) as a function of peak R magnitude. This is a measurement that approximates our efficiency if we had better photometric preselection. We do note that for a fixed amount of galaxy-light contamination it is easier to classify a bright SN Ia than a relatively faint SN Ib/c, indicating that the "Gal" category
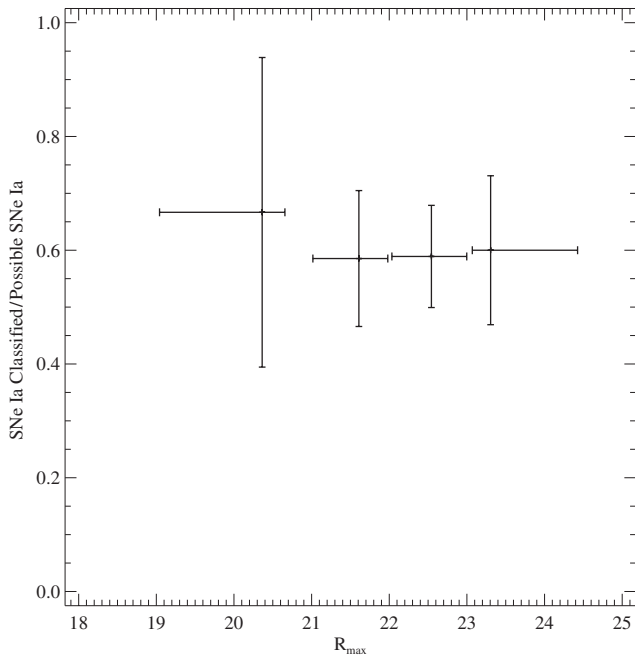
Figure 14. Ratio of the number of SNe Ia classified to the number of total objects which may be SNe Ia (those classified as SNe Ia, SNe Ia?, Gal, Unk, or N.S.) as a function of peak R magnitude. The bins are for objects with $R_{max} < 21$, $21 \leqslant R_{max} < 22$, $22 \leqslant R_{max} < 23$, and $R_{max} > 23$ mag, with the points plotted at the median value for each bin.

may contain a lower fraction of SNe Ia than the survey as a whole.

Although not all objects classified as Unk, for example, are SNe Ia, this ratio still yields a useful approximation of our spectroscopic efficiency as a function of brightness. Note that the ratio is a minimum efficiency since it will increase by either identifying objects as transients other than SNe Ia (by decreasing the number of possible SNe Ia) or by identifying objects as SNe Ia (by increasing the number of SNe Ia).

Regardless of maximum brightness, we appear to identify similar percentages of possible SNe Ia and definite SNe Ia. Therefore, we appear to apply a consistent approach to obtaining sufficient-quality spectra to identify SNe Ia for objects of all brightnesses.

4.2. Sample Demographics

In the local universe, there are many subtypes of SNe Ia. The most common peculiar subtypes are those of SNe 1991T and 1991bg (described in Section 3), corresponding to more and less luminous events, respectively. Li et al. (2001a) found that 20% and 16% of nearby SNe Ia are similar to SNe 1991T and 1991bg, respectively. To determine if the ESSENCE sample of SNe Ia is representative of the full SN Ia population and if the high-redshift population has different demographics from the low-redshift population, we examine the peculiarity rate in the ESSENCE sample.

4.2.1. Peculiar Type Ia Supernova Sample

SNID cross-correlates an SN spectrum with a library of template SN spectra. The template spectra have been classified into subtypes (see Section 3). If > 50% of the best-fit template spectra for a given SN are all part of a particular subtype, then the SN is considered to be of that subtype.

Using SNID, we have determined that five of our SNe Ia (b004, d009, d083, d093, and p534) are SN 1991T-like SNe
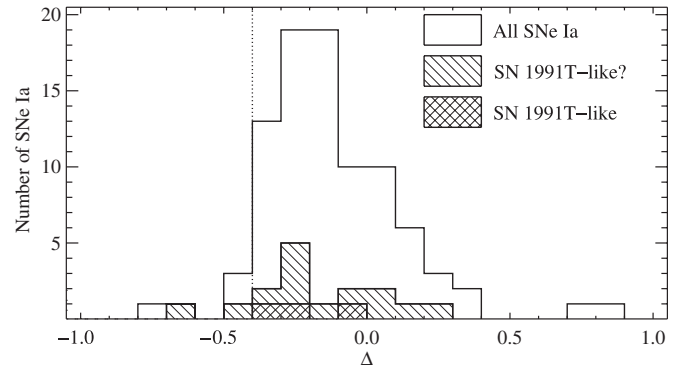

Figure 15. Δ distribution of spectroscopically identified SNe Ia from the first four years of the ESSENCE survey and light curves fit by Wood-Vasey et al. (2007). Subsamples as objects identified by SNID as either being of the subtype consisting of SN 1991T-like objects or having a best-fit template of that subtype are also shown. Increasing Δ corresponds to narrower light curves and less luminous SNe Ia. The dotted line indicates the Δ limit beyond which MLCS has to extrapolate to fit light curves. As such, objects with $\Delta < -0.4$ should be discounted.

Ia. Matheson et al. (2005) also claimed that b004 and d083 are similar to SN 1991T. The light curves of b004 and d009 were not fit by Wood-Vasey et al. (2007); however, d083, d093, and p534 were found to have $\Delta = -0.273$, -0.365, and -0.096, respectively. SN 1991T and the SN 1991T-like SN 1999aa have $\Delta = -0.220$ and -0.271, respectively (Jha et al. 2007).

There are an additional 19 objects which do not pass the threshold necessary to be safely considered as an SN 1991T-like object, but have a best-fit template that is of that subtype. For the sample of 24 SNe Ia that are either classified as SN 1991T-like or have a best-fit template of that subtype, there are 16 objects with light curves fit by Wood-Vasey et al. (2007), having a mean Δ of -0.178. The entire ESSENCE sample with light curves fit by Wood-Vasey et al. (2007) has a mean Δ of -0.121. The Δ distributions of both the entire sample and the subsample of SN 1991T-like objects are shown in Figure 15.

We have also identified a single object (m226) with a best-fit template similar to SN 1991bg, but it did not pass the threshold to be considered SN 1991bg-like. Since no SN 1991bg-like objects have been spectroscopically confirmed at high redshift, we pay particular attention to the classification of this object. There are several reasons why we do not believe m226 should be classified as a SN 1991bg-like object. First, the spectrum only matched three SNID template spectra, two of which were SNe Ia-norm. Second, the best-match template spectrum is of SN 1999gh at 42 d past maximum light, while the light-curve age is 24 d past maximum light. The best-match template with a spectral age near that of the light-curve age of m226 is SN 2002bo (at 29 d past maximum light), which is a SN Ia-norm. Third, SN 1999gh is a low-luminosity SN Ia with a deep Si II $\lambda5800$ line; however, it does not share many of the spectral features of SN 1991bg (Matheson et al. 2008). Fourth, the spectrum of m226 has a relatively low S/N ratio, where proper subtyping is dubious. Finally, the light-curve fit of m226 yielded $\Delta = -0.227$, which is on the opposite end of the Δ range from SN 1991bg-like objects. With all of these data, we are therefore unable to properly classify the subtype of m226.

4.2.2. Peculiarity Rate

The spectral features that distinguish SNe 1991T and 1991bg from SNe Ia-norm can be hidden by low-S/N spectra, spectra with a restricted rest-frame wavelength range, and spectra ob-

tained well after maximum brightness. Nevertheless, we still have observed very few peculiar SNe Ia in the ESSENCE survey. Of the 131 SNe Ia and SNe Ia?, we have spectroscopically confirmed 5 SNe Ia similar to SN 1991T (with 19 additional potential objects). Therefore, we have determined that 4%–19% of the SNe Ia from the ESSENCE survey are similar to SN 1991T, while no ESSENCE SN is similar to SN 1991bg. Because of selection effects (discussed below), our upper limit of SN 1991T-like objects may be lower than the real value; however, since the lower limit is determined by definitive detections, it cannot be smaller. Bronder et al. (2008) spectroscopically confirmed 2–3 high-redshift SNLS SNe Ia out of a sample of 54 to be comparable to SN 1991T; this rate is similar to that found in the ESSENCE survey.

Comparing to low-redshift SN searches, Li et al. (2001a) found that 20% and 16% of nearby SNe Ia are similar to SNe 1991T and 1991bg, respectively. Our raw rate of SN 1991bg-like objects appears to be very low compared to the low-redshift rates. However, with a typical limiting magnitude of $R = 24$ mag, we would only expect to be complete for SN 1991bg-like objects out to $z \approx 0.35$. We have detected 46 SNe Ia (or SNe Ia?) with $z \leqslant 0.35$. If the low-redshift rates are similar to the rates at $z \approx 0.35$, we would expect to have detected 7 SN 1991bg-like SNe Ia in this subsample. If there are no SN 1991bg-like SNe Ia at high redshift, but the ratio of SN 1991T-like to SNe Ia-norm remains constant, then one would expect 24% of high-redshift SNe Ia to be similar to SN 1991T. Considering the selection effects involved, we believe that the rate of SN 1991T-like SNe Ia spectroscopically confirmed in the ESSENCE survey is consistent with the rate found at low redshift. Conversely, we find that the raw rate of SN 1991bg-like SNe Ia found in the ESSENCE survey is low. A further indication of a low raw rate is that no survey has spectroscopically confirmed an SN 1991bg-like SNe Ia at high redshift.

To determine a reasonable detection efficiency for SNe similar to SN 1991bg, we performed a basic simulation. Starting with the maximum-light spectrum of SN 1991bg, we added a varying amount of noise and galaxy contamination (using the spectrum of an elliptical galaxy). We then processed the spectra with SNID, removing SN 1991bg from our sample of template SNe and restricting our wavelength range to 3000–6600 Å, an appropriate rest-frame wavelength for $z = 0.35$. From this, we were able to determine what parameters of S/N and galaxy contamination would yield a correct subtype classification by SNID. We repeated this process for SN 1991T with an Sb galaxy. The results are shown in Figure 16. For this simulation, we did not make any assumption about the SN or host galaxy luminosities. SN 1991bg-like objects should be less luminous and have more luminous host galaxies than SN 1991T-like objects. This would mean that the average spectrum of an SN 1991bg-like object should have more galaxy contamination than that of an SN 1991T-like object.

From Figure 16, we see that for $z \leqslant 0.35$, we should detect essentially all SN 1991T-like objects. However, for SN 1991bg-like objects, the detection efficiency is strongly dependent on galaxy contamination. We would detect most SN 1991bg-like objects with $< 60\%$ galaxy contamination.

If we assume that the low- and high-redshift peculiarity rates are the same, then selection effects and classification systematics must decrease the SN 1991T-like classification rate by a factor of 1–5. Considering that SN 1991bg-like objects tend to be found in high surface-brightness galaxies, many of these objects will be fainter than their galaxies at their position. We are able to
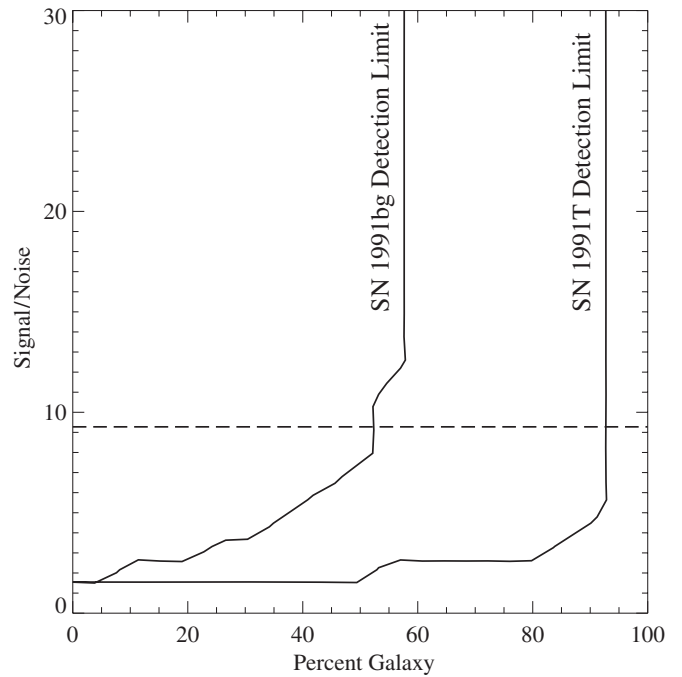

Figure 16. Contours representing the region of S/N-galaxy contamination parameter space that SNe Ia similar to SNe 1991T and 1991bg at $z = 0.35$ will have a correct subtype classification from SNID. We have made no assumption about the relative luminosities of the SNe or host galaxies. If a spectrum is to the upper left of the contour, then it is correctly classified into its subtype. The dashed line is the median S/N for our sample of SNe Ia with $z \leqslant 0.35$. The detection efficiencies show that we should recover nearly every SN 1991T-like SN Ia to this redshift, while the detection of SN 1991bg-like objects is heavily dependent on the amount of galaxy contamination.

remove a significant amount of galaxy light during spectral reductions (particularly for elliptical galaxies where the radial light distribution is smooth), but it is still likely that a significant number of spectra of these objects would be dominated by galaxy light, and therefore would not be classified in this subtype by SNID.

If we assume that most spectra of SN 1991bg-like objects will have galaxy contaminations of 25%–75% and a S/N of 4–15 (similar to most of our spectra), we can determine the percentage of these spectra that SNID would classify as SN 1991bg-like objects. Placing these constraints in the parameter space shown in Figure 16, we see that 54% of the remaining parameter space results in a positive detection.

If we assume that the selection effects and classification systematics are essentially equal to the detection efficiency of SNID given our assumed parameters above, we require a bias factor of 1.86 for the SN 1991bg-like objects compared to the SN 1991T-like objects. Using this factor, we would expect the SN 1991bg-like peculiarity rate to be 2%–8% for the ESSENCE sample. This corresponds to 1–4 SNe in our $z \leqslant 0.35$ sample, consistent with our non-detection of SN 1991bg-like events in our sample. Increasing the sample size and constraining the bias factors will greatly improve the constraints.

A secondary method to examine the rate of SN 1991bg-like objects is by measuring the light-curve shapes of our SNe Ia. SN 1991bg-like objects have significantly different light-curve shapes than normal SNe Ia, with corresponding $\Delta > 1$. Our sample contains 31 SNe Ia with $z \leqslant 0.35$ and Δ information. If the local rate of SN 1991bg-like objects is constant to $z = 0.35$, then we would expect to have 5 SN 1991bg-like objects in this

sample. None of the SNe Ia in this sample have $\Delta > 1$. Assuming that all objects spectroscopically similar to SN 1991bg also have $\Delta > 1$, the nondetection of any of these objects is 2.2σ from the expected value.

A significant bias against classifying SN 1991T-like SNe Ia (particularly objects similar to SN 1999aa) at high redshift is that their post-maximum spectra are very similar to those of SNe Ia-norm. For instance, there is essentially no difference between the spectra of the normal SN 1994D and SN 1999aa one week after maximum brightness (Garavini et al. 2004). Therefore, for a large percentage of our SNe Ia, we have no real constraint on the peculiarity of the individual object. More detailed modeling is necessary to determine the classification success as a function of phase, S/N, and wavelength range of a particular spectrum.

5. CONCLUSIONS

We have presented optical spectra of targets selected for follow-up observations during the first four years of the ESSENCE survey. We have shown that as the survey matured, we were able to detect more SNe Ia at higher redshifts and at later phases without reducing efficiency for a total of 127 SNe Ia and possible SNe Ia ("Ia?"). There were more SNe Ia observed in the second two years than in the first two years, showing that we are on track to reach the goal of the ESSENCE survey: constraining the equation-of-state parameter of dark energy to $\lesssim 10\%$ by observing ~ 200 SNe Ia over the redshift range $0.2 \lesssim z \lesssim 0.8$.

The spectra of the ESSENCE high-redshift SNe Ia are broadly consistent with those of their low-redshift counterparts; see Foley et al. (2008) for a detailed comparison of composite spectra made from this sample. If the ESSENCE SNe Ia were drastically different from their local counterparts, then the correlations of redshift and age found by SNID would have larger scatter. We are able to automatically classify the majority of our objects using SNID. However, human intervention, through visual inspection or using a second fitting program, was necessary to properly classify several objects. SNID is able to accurately quantify the redshift and phase determination for our sample of SNe Ia. The peculiarity rate of the spectroscopically distinct SN 1991T-like and SN 1991bg-like objects are consistent with low-redshift rates. None of our spectra or light curves fit by Wood-Vasey et al. (2007) are similar to the spectroscopically peculiar SN 1991bg, but if considering systematic effects, at a rate that is consistent with low-redshift rates.

REFERENCES

Allington-Smith, J., et al. 1994, PASP, 106, 983
Appenzeller, I., et al. 1998, Messenger, 94, 1
Astier, P., et al. 2006, A&A, 447, 31
Balland, C., et al. 2007, A&A, 464, 827
Barris, B. J., & Tonry, J. L. 2004, ApJ, 613, L21
Blondin, S., & Tonry, J. L. 2007, ApJ, 666, 1024
Blondin, S., Walsh, J. R., Leibundgut, B., & Sainton, G. 2005, A&A, 431, 757
Blondin, S., et al. 2006, AJ, 131, 1648
Blondin, S., et al. 2008, ApJ, 682, 724
Branch, D., Fisher, A., & Nugent, P. 1993, AJ, 106, 2383
Bronder, T. J., et al. 2008, A&A, 477, 717
Davis, T. M., et al. 2007, ApJ, 666, 716
Dressler, A., Hare, T., Bigelow, B. C., & Osip, D. J. 2006, in Proc. SPIE 6269, Ground-based and Airborne Instrumentation for Astronomy, ed. I. S. McLean & M. Iye (Bellingham, WA: SPIE), 62690F
Ellis, R. S., et al. 2008, ApJ, 674, 51
Faber, S. M., et al. 2003, in Proc. SPIE 4841, Instrument Design and Performance for Optical/Infrared Ground-based Telescopes, ed. Masanori Iye, Alan F. M. Moorwood (Bellingham, WA: SPIE), 1657
Fabricant, D., Cheimets, P., Caldwell, N., & Geary, J. 1998, PASP, 110, 79
Filippenko, A. V. 1988, AJ, 96, 1941
Filippenko, A. V. 1997, ARA&A, 35, 309
Filippenko, A. V. 2005, in Astrophysics and Space Science Library 332, White Dwarfs: Cosmological and Galactic Probes, ed. E. M. Sion, S. Vennes, & H. L. Shipman (Dordrecht: Springer), 97

Filippenko, A. V., Matheson, T., & Ho, L. C. 1993, ApJ, 415, L103+
Filippenko, A. V., et al. 1992a, AJ, 104, 1543
Filippenko, A. V., et al. 1992b, ApJ, 384, L15
Foley, R. J., et al. 2008, ApJ, 684, 68
Foley, R. J., et al. 2003, PASP, 115, 1220
Galama, T. J., et al. 1998, Nature, 395, 670
Garavini, G., et al. 2004, AJ, 128, 387
Garavini, G., et al. 2007, A&A, 470, 411
Glazebrook, K., & Bland-Hawthorn, J. 2001, PASP, 113, 197
Guy, J., et al. 2007, A&A, 466, 11
Hook, I. M., Jørgensen, I., Allington-Smith, J. R., Davies, R. L., Metcalfe, N.,
     Murowinski, R. G., & Crampton, D. 2004, PASP, 116, 425
Horne, K. 1986, PASP, 98, 609
Howell, D. A., et al. 2005, ApJ, 634, 1190
Jha, S., Riess, A. G., & Kirshner, R. P. 2007, ApJ, 659, 122
Kowalski, M., et al. 2008, ApJ, 686, 749
Leibundgut, B., et al. 1993, AJ, 105, 301
Li, W., Filippenko, A. V., Treffers, R. R., Riess, A. G., Hu, J., & Qiu, Y.
     2001a, ApJ, 546, 734
Li, W., et al. 2001b, PASP, 113, 1178
Li, W., et al. 2003, PASP, 115, 453

Matheson, T., Filippenko, A. V., Ho, L. C., Barth, A. J., & Leonard, D. C.
     2000, AJ, 120, 1499
Matheson, T., et al. 2005, AJ, 129, 2352
Matheson, T., et al. 2008, AJ, 135, 1598
Miknaitis, G., et al. 2007, ApJ, 666, 674
Oke, J. B., et al. 1995, PASP, 107, 375
Perlmutter, S., et al. 1999, ApJ, 517, 565
Phillips, M. M. 1993, ApJ, 413, L105
Phillips, M. M., Wells, L. A., Suntzeff, N. B., Hamuy, M., Leibundgut, B.,
     Kirshner, R. P., & Foltz, C. B. 1992, AJ, 103, 1632
Poznanski, D., et al. 2007, MNRAS, 382, 1169
Riess, A. G., Press, W. H., & Kirshner, R. P. 1996, ApJ, 473, 88
Riess, A. G., et al. 1998, AJ, 116, 1009
Riess, A. G., et al. 2007, ApJ, 659, 98
Schmidt, G. D., Weymann, R. J., & Foltz, C. B. 1989, PASP, 101, 713
Strolger, L.-G., et al. 2002, AJ, 124, 2905
Tonry, J. L., et al. 2003, ApJ, 594, 1
Turatto, M. 2003, in Lecture Notes in Physics 598, Supernovae and Gamma-Ray
     Bursters, ed. K. Weiler (Berlin: Springer), 21
Wade, R. A., & Horne, K. 1988, ApJ, 324, 411
Wood-Vasey, W. M., et al. 2007, ApJ, 666, 694